# DYNAMICS AND CONTROL OF JUMPING LEGGED ROBOT

by

GURASHISH SINGH

Presented to the Faculty of the Graduate School of

The University of Texas at Arlington in Partial Fulfillment

of the Requirements

for the Degree of

MASTER OF SCIENCE IN

MECHANICAL ENGINEERING

THE UNIVERSITY OF TEXAS AT ARLINGTON

MAY 2018

Acknowledgements

I take this opportunity to thank my supervising professor Dr. Alan Bowling for allowing me to join his research lab - Robotics, Biomechanics and Dynamic System laboratory – and his instrumental advice during the course of my master's Thesis. There were times when I was stuck and was not getting results, but Dr. Bowling's support never faltered. I also thank my thesis committee members, Dr. Kamesh Subbarao and Dr. Daejong Kim for taking out time from their busy schedule and bearing with me rescheduling my defense.

I also thank all the members of The Robotics, Biomechanics and Dynamic System Laboratory, Abhishek Chatterjee, for all his indispensable help without which I couldn't have pushed past certain hurdles, Vatsal Joshi, helping me debug when I was stuck for days, Dr. Ashley Guy, for his timely inputs, Manoochehr Rabiei, for his all-knowing tirades about the world, Eric Havenhill, for all the times he helped me get some Tapioca tea, Iretomiwa Esho , Regan Kubicek and Luke Oliver, for being some great lab colleagues.

I would also like to thank Denish Baman, Ravi Patel, Samson and Omar for all their help. Pooja Sridhar, Himanshi Tulsani and Sanchit Puri, thank you for always being there for me.

Finally, my parents, without their blessings I would not be here. Thank you.

May,24 2018

# Abstract

DYNAMICS AND CONTROL OF JUMPING LEGGED ROBOT

GURASHISH SINGH MS

The University of Texas at Arlington, 2018

Supervising Professor: Alan Bowling

This research aims at studying the agility of legged robots particularly their interactions with the ground and achieve a jumping motion by using an operational space controller.

Methods were developed to first formulate the equations of motions of the full system. Then we used the published impact and contact analytical framework to detect simultaneous, indeterminate impact and transition to contact with friction and addressed the well-known issues with energy consistency when using rigid body models for dynamic systems (i.e. there are no unusual gains in the energy after impact has ended). Non-penetration of the ground was achieved through online constraint embedding where degrees of freedom were reduced as any point came in to contact with the ground. Finally, operational space control was used to control the motor torques of the legged robot that would lift the foot off of the ground and simulate a jumping motion.

Table of Contents

Acknowledgements ..... iii

List of Illustrations ..... vii

Chapter 1 Introduction ..... 1

1.1 Overview ..... 1

1.2 Motivation ..... 3

1.3 Research Contributions ..... 3

Chapter 2 Dynamic Simulation ..... 4

2.1 Rigid Body Simulation ..... 4

2.2 Complementarity Conditions ..... 6

2.3 Collision Detection ..... 7

Chapter 3 Impact and Contact Analysis ..... 10

3.1 Impact Analysis ..... 10

3.2 End of Impact Energy Analysis ..... 12

3.3 Contact Analysis ..... 13

3.3.1 Reaction forces during contact ..... 14

Chapter 4 Operational Space Control ..... 18

4.1 Operational Space Equation Formulation ..... 18

4.1.1 If the Task Jacobian $Jx$ is invertible ..... 19

4.1.2 If the Task Jacobian $Jx$ is not invertible ..... 20

4.1.3 If $(Jx(KTAK) - 1KTGT)$ is not a square matrix ..... 20

4.1.4 Using the Dynamically Consistent Generalized Inverse of Jacobian ..... 20

Chapter 5 Results ..... 22

5.1 Simulation Technique ..... 22

5.2 Simulation Example ..... 22
5.3 Energy and Torque Plots ..... 24
Chapter 6 Conclusion ..... 29
References ..... 30
Biographical Information ..... 31

List of Illustrations

Figure 1-1: Planar model of a leg……1

Figure 2-1: Pre- and Post-impact regions for impact modeling..……4

Figure 2-2: Friction cone based on theory of Coulomb friction……...……...…6

Figure 2-3: Flow process used for impact and contact simulations...……..9

Figure 5-1: Planar Model of a Leg…….23

Figure 5-2: Total energy after First Impact event…..……..…….……..…24

Figure 5-3: Torques leading up to the lift……..……..……25

Figure 5-4: Total Energy Plot……..26

Figure 5-5: Motion Capture of the foot lifting off the ground…….....27

Figure 5-6: Motion Capture of the whole model…..……..…28

# Chapter 1

# Introduction

## 1.1 Overview

The goal of this research is aimed at studying the agility of legged robots especially interactions with the ground by considering factors such as impact and contact with the ground, friction and restitution. Robots must be able to rapidly adapt to the various changes in the environment without human interference. Agility of a robot, for instance, may refer to it jumping over an obstacle in its path in a controlled manner by adjusting its acceleration while maintaining static (the ability to retain the centre of mass above the base of support in a stationary position) and dynamic (the ability to maintain balance with body movement) balance.

A 2-dimensional 4-link robot is modelled in this research with the first three links being the Foot, Tibia and Femur while the fourth link is signified as the rest of the body (Figure 1-1).

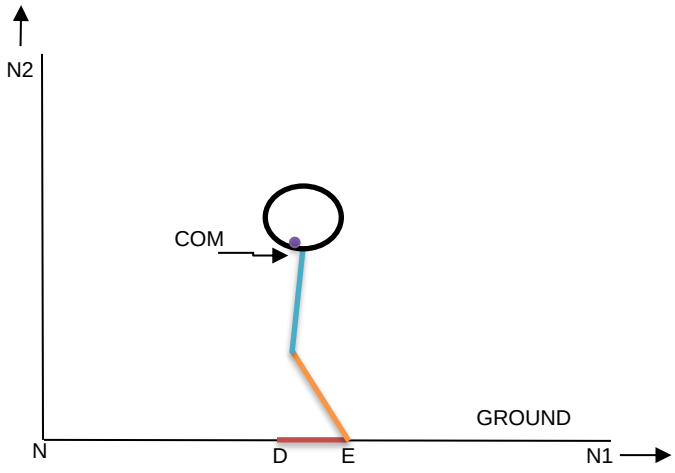


Figure 1-1: Planar model of a leg

All the links are considered as rigid bodies and any local deformation due to impact is considered negligible. Here, impact is decided as an abrupt reaction between colliding bodies and contact is established as a succession of impacts. The mechanics of collisions deal with stress, displacement (i.e. local indentation) and wave propagation of forces, which are not considered in this research.

This research is focused on dynamic simulation of the ground interactions of the legged robot and to see whether it can lift off the ground by applying appropriate torque to the links in a controlled manner, while taking into consideration the forces, impulses, velocities and frictions related to the impact or contact points. This research uses a recently published framework to use an energetically consistent model of impact and contact which will address sticking and slipping for various contact points with friction. Arbitrary energy gains upon impact with the ground and feasibility of post-impact velocities, if any, will also be assessed. The indeterminate nature of the system equations of motion is one of the key issues in this research. The indeterminacy is due to the multiple points experiencing impact or contact simultaneously.

The system's equations of motion are determined using Kane's method with the help of a software called Autolev. Impact/contact detection takes place using the velocities and accelerations of the points in impact/contact. Impulse-Domain analysis is used to calculate post-impact velocities or the rebound velocities. Stick-slip analysis is done during the impulse-domain analysis to check for any slip-reversals (Chapter 3). Non-penetration of the ground is achieved by reduction in the equations of motion by restricting the normal component of the velocities of the points in contact and hence reduction in the degrees of freedom. Frictional constraints are also enforced at this stage. New generalized speeds and accelerations are found out using the reduced equations of motion. To make the foot lift off the ground, we use operational space control to find out

the motor torques at each joint. Using the gear torque ratios, we choose the appropriate motor torques. In this research, we provide the desired positions of the system's centre of mass while keeping desired velocities and accelerations as zero.

## 1.2 Motivation

The motivation for our research is to implement the established impact and contact analytical framework and use the operational space torque to get a realistic lift off of the foot in our dynamic model.

## 1.3 Research Contributions

In Chapter 2, we'll talk briefly about what constitutes an impact and contact. Also, we'll look at Coulomb friction and the complementarity conditions.

In Chapter 3, we'll analyse the impulse-domain and time-domain calculations, the switching of models between freefall, multi-point impact and contact analysis, and also the energetic termination of impacts.

In Chapter 4, we look at the operational space control equation formulation and the problems faced when the Jacobian matrix is not square.

In Chapter 5, we show our simulation results and go into more detail about how we arrived at the said results.

# Chapter 2

# Dynamic Simulation

## 2.1 Rigid Body Simulation

To gain a better understanding about the robot and ground interactions, impact and contact modelling needs to be understood. This chapter introduces rigid body impact dynamics simulation where event-based, adaptive integration is used to determine the dynamics of the system, especially near times where contact states change and the online embedding constraint technique used to model contacts. Rigid body impacts are characterized by quick changes in the system velocities and presence of large forces on the bodies.

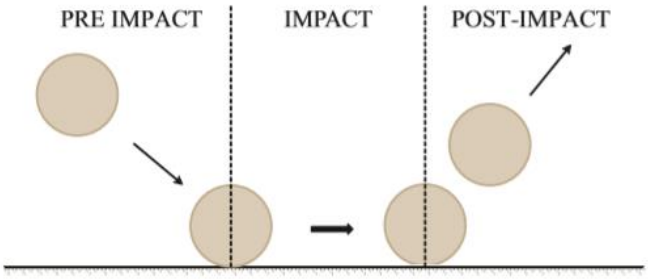


Figure 2-1: Pre- and Post-impact regions for impact modeling

Contact is referred to as a body touching the surface of the ground. A force is present at the point where the body and ground coincide. Impact is defined as contact with abrupt velocity changes.

Here, rigid body impacts are modelled as discrete events using a discontinuous approach as shown in figure 2-1 [1]. It is assumed that the impact event occurs over a very short time in which the position and orientation of the system remains constant,

which establish the Darboux-Keller impact dynamics [2]. Here, contact is treated as a succession of discrete impact events. This approach, also referred to as piecewise [3] or non-smooth [5-7], treats the impact event as an instantaneous change in velocities of the impacting bodies. The post-impact velocities are resolved based on impulse-momentum theory with the help of constraints as shown in [8]. The hybrid or impact and continuous [4], approaches treat the impact event as discontinuous in time-domain but continuous in impulse-domain [9–11]. The hybrid approach is used in this work.

This research makes use of an already developed analytical framework for the treatment of simultaneous, multi-point impact problems in the presence of friction. Coulomb friction is used in the framework developed to relate the tangential impulse to the normal impulse by a coefficient of friction (COF) [12]. This relationship can be visualized using the friction cone for Coulomb friction, depicted in Fig. 2-2. The friction force may be discontinuous because changes in the friction direction during an impact event can occur due to sliding or sticking – a dynamic, μd or static, μs, COF may be used, respectively. The inner region of the friction cone represents sticking, whereas the outer region is sliding. The boundary of the friction cone between these two regions is the stick-slip transition where an impact point with initial sliding comes to rest and then resumes slip, slip-reverses or remains in the stick region [13,14]. The lower bound on COF which induces sticking is represented by the critical COF, $\bar{\mu}$.

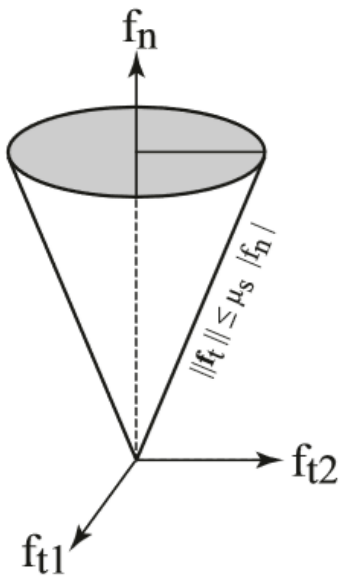


Figure 2-2: Friction cone based on theory of Coulomb friction

## 2.2 Complementarity Conditions

The complementarity conditions define a relationship between friction, contact forces, velocities and accelerations [15]. The complementarity conditions are dependent on the value of the pre-impact normal velocities and accelerations, $v_{ni}$(t) and $\dot{v}_{ni}$(t), assuming the distance between the impacting points equals zero.

$$\begin{cases} if & \boldsymbol{v_{ni}}(t) & < & -\epsilon_v & and & \dot{\boldsymbol{v}}_{\boldsymbol{ni}}(t) & < & 0 & impact(impulse-domain\ analysis) \\ if & |\boldsymbol{v_{ni}}(t)| & < & \epsilon_v & and & \dot{\boldsymbol{v}}_{\boldsymbol{ni}}(t) & < & 0 & contact(constrain\ embedding) \\ if & \boldsymbol{v_{ni}}(t) & > & \epsilon_v & or & \dot{\boldsymbol{v}}_{\boldsymbol{ni}}(t) & > & 0 & seperation(floating-base\ EOM) \end{cases} \quad (2.1)$$

A transition between impact and contact occurs when the pre-impact normal velocity equals zero. Further, the pre-impact acceleration must be checked to determine whether impact forces exist or not. According to classical Coulomb friction, the post-impact tangential velocities satisfy,

$$\begin{cases} \boldsymbol{v_{ti}} = 0 \;\; and \;\; \dot{\boldsymbol{v}}_{\boldsymbol{ti}} = 0 \;\; then \;\; |\boldsymbol{f_{ti}}| \leq \mu_s |\boldsymbol{f_{ni}}| \;\; sticking \\ \boldsymbol{v_{ti}} = 0 \;\; and \;\; \dot{\boldsymbol{v}}_{\boldsymbol{ti}} \neq 0 \;\; then \;\; |\boldsymbol{f_{ti}}| = \mu_s |\boldsymbol{f_{ni}}| \;\; stick - slip \; transition \\ \boldsymbol{v_{ti}} \neq 0 \;\; and \;\; \boldsymbol{v_{ti}} \neq 0 \;\; then \;\; |\boldsymbol{f_{ti}}| = \mu_d |\boldsymbol{f_{ni}}| \;\; slipping \end{cases} \quad (2.2)$$

where, $\mu_s \; and \; \mu_d$ are the static and dynamic coefficients of friction [15].

The no-slip condition is defined by the first relation in (2.2), the stick-slip transition is defined by the second, and slipping, or sliding is defined by the third. In (2.2) there is a discontinuous change in the coefficient of friction, assuming μs = μd, and thus a discontinuous change in the friction forces. This discontinuity defines an abrupt transition from sticking to slipping

The relationships in Eqns. (2.1) and (2.2) are the basis for what is referred to as a complementarity problem [16]. The complementarity conditions apply to both contact and impact forces independently. In this work, the impulsive forces are used to check the no-slip condition. The complementarity conditions in terms of impulses are presented in [17],

$$\begin{cases} \boldsymbol{v_{ti}} = 0 \;\; and \;\; \dot{\boldsymbol{v}}_{\boldsymbol{ti}} = 0 \;\; then \;\; |p_{ti}| \leq \mu_s |p_{ni}| \;\; sticking \\ \boldsymbol{v_{ti}} = 0 \;\; and \;\; \dot{\boldsymbol{v}}_{\boldsymbol{ti}} \neq 0 \;\; then \;\; |p_{ti}| = \mu_s |p_{ni}| \;\; stick - slip \; transition \\ \boldsymbol{v_{ti}} \neq 0 \;\; and \;\; \dot{\boldsymbol{v}}_{\boldsymbol{ti}} \neq 0 \;\; then \;\; |p_{ti}| = \mu_d |p_{ni}| \;\; slipping \end{cases} \quad (2.3)$$

## 2.3 Collision Detection

In this research, an event-driven scheme, similar to [18,19] in conjunction with MATLAB's ode45 integrator stops the simulation when a collision is detected. This approach is used to treat the impact events and determine the post-impact velocities of the system. These velocities serve as the initial conditions when the simulation is restarted. This technique is followed herein each time a collision is detected in the simulations conducted.

The process flow chart presented in Figure 2-3 illustrates the operations performed during a typical simulation. We start the simulation with some initial conditions. As we are using an event-based simulation technique, if any point encounters the contact surface, the event function is called, and our simulation is stopped. Eq. (2.1) is used to check if the point experiences an impact or not. If the point experiences impact, we move onto impulse-domain analysis (further explained in chapter 3). In the hybrid dynamic simulation of rigid bodies, when a rigid body touches a contact surface but does not rebound, which leads to a successive series of impact events that, in effect, stop the time domain simulation. Such a no-rebound condition is referred to as contact. Online constraint-embedding techniques are used to enforce non-penetrability constraints and frictional constraints to ensure that the point does not penetrate the ground and that there is no slip. Coordinate reduction techniques such as QR decomposition method has been used in this research to reformulate the equations of motion based on a minimal set of independent generalized coordinates. Once contact has been achieved, operational space control is used to calculate the desired motor torques.

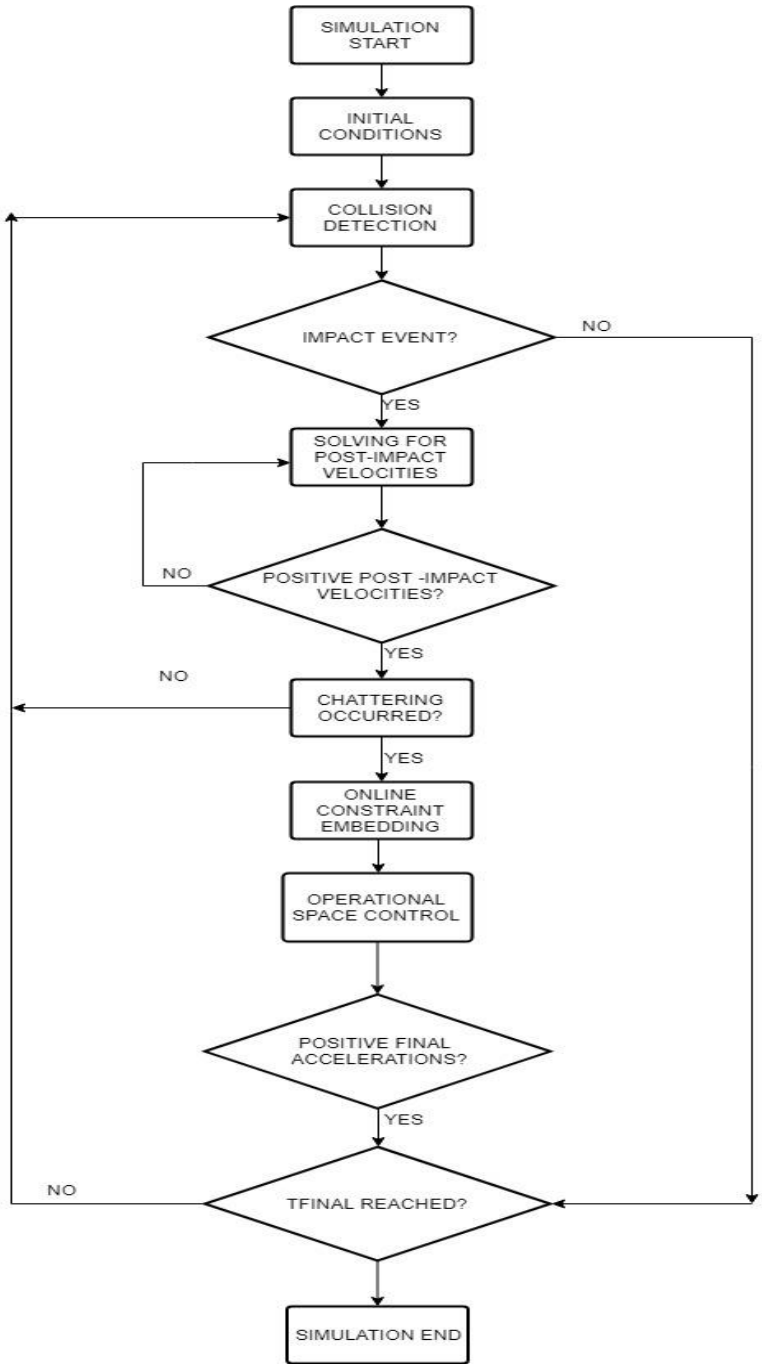


Figure 2-3: Flow process used for impact and contact simulations

# Chapter 3

## Impact and Contact Analysis

The previously published framework for simultaneous, multiple point impact with friction has been used in this research which yield equations of motion that are indeterminate with respect to the impact forces and a no-rebound contact represented by smooth dynamics where non-penetrability conditions along with frictional constraints are enforced in this work[21]. This chapter will provide a brief overview of impact and contact analysis.

### 3.1 Impact Analysis

Our dynamic model is a 4 link and 6 DOF system. A general form of the equations of motion for the system can be expressed as:

$$A\ddot{\boldsymbol{q}} + b(\dot{\boldsymbol{q}}, \boldsymbol{q}) + g(\boldsymbol{q}) = \boldsymbol{\Gamma} = J^T(\boldsymbol{q})\boldsymbol{F} + G^T\boldsymbol{\gamma} \tag{3.1}$$

where,

$$\boldsymbol{F} = [f_{t1}\ f_{n1}\ f_{t2}\ f_{n2}\ f_{t3}\ f_{n3}\ f_{t4}\ f_{n4}\ f_{t5}\ f_{n5}]^T \tag{3.2}$$

and A is the mass matrix for the system. b and g define the Coriolis and gravity terms respectively. The generalized active forces are represented by **Γ** and are related to the impact forces, **F**, through the impact Jacobian matrix, $J$. $G^T$ is the Gear Ratio matrix that picks out the corresponding motor torques from the vector $\boldsymbol{\gamma}$. The above equation can be integrated over an infinitesimally small time-period which will convert the equation from a force-based to an impulse-based one. The equation of motion of the system, in impulse-domain then becomes:

$$\dot{\boldsymbol{q}} = \dot{\boldsymbol{q}}(0) + A^{-1}J^T\boldsymbol{p} \tag{3.3}$$

where $\dot{\boldsymbol{q}}(0)$ and $\dot{\boldsymbol{q}}$ refer to the pre- and post-impact generalized speeds of the system.

.

Considering a two point contact, pre-multiplying eq. (3.3) with the impact Jacobian we can obtain the operation-space velocities of the impact points. Hence,

$$\boldsymbol{v} = [v_{t1} v_{n1} v_{t2} v_{n2}]^T = \boldsymbol{v}(0) + JA^{-1}J^T\boldsymbol{p} \tag{3.4}$$

where $\boldsymbol{v}(0)$ and $\boldsymbol{v}$ stand for the pre- and post-impact velocities of the impact points. The tangential and normal velocities of the impact points are represented by $v_{ti}$ and $v_{ni}$ respectively, where i = 1,2. In Eq. (3.4), **p** =$[p_{t1}\ p_{n1}\ p_{t2}\ p_{n2}\ ]^T$ represents all the impulses at different contact points. The impulses in p can be resolved in terms of one arbitrarily chosen independent impulse parameter,

$$\boldsymbol{p} = \boldsymbol{C}p_{n2} \quad where\ p_{n2} \geq 0 \tag{3.5}$$

The coefficient **C**, which depends upon the slip-state of the various contact points, is derived using frictional and rigid-body constraints . Hence, using Eq. (3.3) and Eq. (3.5) the contact point velocities $v$ during an impact event may be expressed as,

$$\boldsymbol{v} = \boldsymbol{v}(0) + JA^{-1}J^T\boldsymbol{C}p_{n2}\ where\ p_{n2} \geq 0 \tag{3.6}$$

Eq. (3.6) may be rewritten as,

$$\boldsymbol{v} = \boldsymbol{v_k} + JA^{-1}J^T\boldsymbol{C}(p_{n2} - p_{sk})\ \ where\ \ p_{n2} \geq 0 \tag{3.7}$$

where, $p_{sk}$ is the value of the independent impulse parameter, $p_{n2}$ at $k^{th}$ stick-slip transition, $\boldsymbol{v}_k$ is the velocities at the various stick-slip transitions where the subscript k = 0,1,2,..,N refer to the stick-slip transitions, including the pre-impact velocities $\boldsymbol{v_0} = \boldsymbol{v}(0)$. Stick-slip analysis is done for the point(s) whose tangential velocities reach zero. Such point(s) may remain sticking ($\boldsymbol{v_t} = 0$) or have a slip-reversal where the point(s) start sliding after coming reaching zero tangential velocity.

## 3.2 End of Impact Energy Analysis

The energy loss for an impact can be attributed to the net work done during compression and restitution (relaxation) phases a body undergoes during impact. In this research the termination of impact events is based on Stronge's Hypothesis on rigid impacts. Stronge's hypothesis defines an energetic coefficient of restitution (ECOR) which incorporates work-energy theory and often leads to energetically consistent results in rigid body impact modelling.

Stronge's hypothesis places an energetic constraint on the evolution of the contact point velocities as a function of the independent impulse parameter as shown in Eq. (3.7). The work done during an impact event is given by the difference in kinetic energy between the pre- and post-impact states of the rigid body system, which is given by

$$W = \frac{1}{2}\dot{\boldsymbol{q}}^T A \dot{\boldsymbol{q}} - \frac{1}{2}\dot{\boldsymbol{q}}^T(0) A \dot{\boldsymbol{q}}(0) \tag{3.8}$$

$$= \frac{1}{2}\boldsymbol{v}^T (J^+)^T A (J^+)\boldsymbol{v} - \frac{1}{2}\boldsymbol{v}^T(0)(J^+)^T A (J^+)\boldsymbol{v}(0) \tag{3.9}$$

where $J^+$ is the pseudo-inverse of the impact Jacobian matrix J. Since, the pre- and post-impact generalized speeds or contact point velocities depend upon independent impulse $p_{n2}$, the work itself becomes a function of the independent impulse parameter.

By using eq. (3.7) and substituting it in eq. (3.9), we can solve for the normal work as a function of the independent impulse $p_{n2}$ :

$$W_n(p_{n2}) = W_{nk} + a(p_{n2} - p_{sk})^2 + b(p_{n2} - p_{sk}) \tag{3.10}$$

where $a$ and $b$ are the constant coefficients. These constant coefficients define the parabolic curve for normal work for a given phase following stick-slip transition k. a and b are dependent upon C but are independent of the initial velocities $p_{n2}$. $W_{nk}$ are the normal work at stick-slip transitions k = 0,1,2,.., N, such that $W_{n0}$ = 0.

According to Stronge's Hypothesis, the energy change during an impact takes place over two consecutive energetic phases: a compression phase followed by a restitution phase. The terminal normal work $W_{nf}$ is related to the normal work at the end of the compression phase $W_{nc}$ as,

$$W_{nf} = (1 - e_*^2)W_{nc} \tag{3.11}$$

Where $W_{nc}$ is the normal work at the end of compression phase and $e_* \in [-1,1]$ is defined as the Global Energetic Coefficient of Restitution which accounts for the energy dissipated during an impact event. The global ECOR $e_*$, describes an energetic relationship between compression and restitution for a single contact point.

## 3.3 Contact Analysis

One of the difficulties encountered with the event-based simulation approach is the accumulation of events due to high frequency chattering behaviour for low-speed contacts. In the hybrid dynamic simulation of rigid bodies, chattering takes place when a rigid body touches a contact surface but does not rebound, which leads to a successive series of impact events that, in effect, stop the time domain simulation.

A no-rebound contact represented by smooth dynamics where non-penetrability conditions along with frictional constraints are enforced in this work. During multiple point contact, rigid body constraints are used along with the frictional constraints.

The criteria used for distinguishing between impact, contact and separation is:

$$\begin{cases} if & \boldsymbol{v_{ni}}(t) < -\epsilon_v & and & \dot{\boldsymbol{v}}_{\boldsymbol{ni}}(t) < 0 & impact(impulse - domain\ analysis) \\ if & |\boldsymbol{v_{ni}}(t)| < \epsilon_v & and & \dot{\boldsymbol{v}}_{\boldsymbol{ni}}(t) < 0 & contact(constrain\ embedding) \\ if & \boldsymbol{v_{ni}}(t) > \epsilon_v & or & \dot{\boldsymbol{v}}_{\boldsymbol{ni}}(t) > 0 & seperation(floating - base\ EOM) \end{cases} \tag{3.12}$$

where $\epsilon_v$ is a small threshold value selected to determine if the contact points have near zero values.

We used online constraint embedding with coordinate reduction techniques to reformulate the equations of motion based on a minimal set of independent generalized coordinates. We first enforced non-penetrability and sticking friction constraints along with rigid body constraints (for multi-point contacts) to compute the reaction forces. The reaction forces were checked using the friction cone defined by Coulomb's law to identify contact points that are slipping. Finally sliding frictional constraints were enforced for the relevant points.

*3.3.1 Reaction forces during contact*

During a no-rebound phase, all the points satisfying the contact criterion in Eq. (3.12) are assumed to stick. Therefore, both the tangential and the normal components are constrained to be equal to zero.

Consider the velocities and accelerations of the contact points that satisfy the contact constraint in Eq. (3.12),

$$0 = \boldsymbol{v_c} = \begin{bmatrix} v_{t_1} \\ v_{n_1} \\ . \\ . \\ . \end{bmatrix} = J_c \dot{\boldsymbol{q}} \tag{3.13}$$

and

$$0 = \dot{\boldsymbol{v}}_{\boldsymbol{c}} = \begin{bmatrix} \dot{v}_{t_1} \\ \dot{v}_{n_1} \\ . \\ . \\ . \end{bmatrix} = J_c \ddot{\boldsymbol{q}} + \dot{J}_c \dot{\boldsymbol{q}} \tag{3.14}$$

where $J_c$ is the Jacobian matrix associated with $\boldsymbol{v_c}$.Substituting the expression for $\ddot{\boldsymbol{q}}$ from Eq. (3.1),

$$0 = \dot{\boldsymbol{v}}_c = J_c A^{-1} {J_c}^T \boldsymbol{F} + J_{\boldsymbol{c}} A^{-1} G^T \boldsymbol{\gamma} - J_c A^{-1} \big(\boldsymbol{b}(\boldsymbol{q}, \dot{\boldsymbol{q}}) + \boldsymbol{g}(\boldsymbol{q})\big) + \dot{J}_c \dot{\boldsymbol{q}} \tag{3.15}$$

Similar to the impulse-domain analysis, the contact forces **F** are going to be constrained by the rigid-body constraints and frictional constraints. Hence the contact constraint forces may be resolved as

$$\boldsymbol{F} = \boldsymbol{C}F_r \tag{3.16}$$

where $F_r$ is an independent force parameter. The vector **C** is computed similar to the impulse-domain analysis.

Now substituting Eq. (4.5) into Eq. (4.4), we get

$$\bar{\boldsymbol{c}}F_r = J_c A^{-1} J_c{}^T \boldsymbol{C}F_r = J_c A^{-1}\big(\boldsymbol{b}(\boldsymbol{q},\dot{\boldsymbol{q}}) + \boldsymbol{g}(\boldsymbol{q})\big) - \dot{J}_c\dot{\boldsymbol{q}} - J_c A^{-1} G^T \boldsymbol{\gamma} \tag{3.17}$$

Hence, the full set of reaction forces **F** would be given by

$$\boldsymbol{F} = \boldsymbol{C}F_r = \boldsymbol{C}\frac{\bar{\boldsymbol{c}}^{\boldsymbol{T}}}{\bar{\boldsymbol{c}}^{\boldsymbol{T}}\bar{\boldsymbol{c}}}\big(J_c A^{-1}\big(\boldsymbol{b}(\boldsymbol{q},\dot{\boldsymbol{q}}) + \boldsymbol{g}(\boldsymbol{q})\big) - \dot{J}_c\boldsymbol{q} - J_c\dot{A}^{-1} G^T \boldsymbol{\gamma} \tag{3.18}$$

The reaction forces in **F** in Eq. (3.18) are calculated assuming that all the points are sticking. Now Coulomb's law is used to check whether the contact points stick or slip,

$$\left|f_{t_i}\right| \le \mu_s f_{n_i} \tag{3.19}$$

where $\mu_s$ is the coefficient of static (limiting) friction. A contact point sticks if equation Eq. (3.19) is satisfied, otherwise the point slips. When a contact point slips, the contact-plane tangential velocities have unknown non-zero values. Thus, the velocity and acceleration constraint in Eqs. (3.13) and (3.14) need to be restricted to only the normal components for the slipping points.

Enforcing the slip and no-slip constraints is accomplished by partitioning the reaction forces as follows:

$$\boldsymbol{F} = \begin{bmatrix}\boldsymbol{F}_{slip}\\ \boldsymbol{F}_{stick}\end{bmatrix} = S_c \begin{bmatrix}\boldsymbol{F}_{slip_n}\\ \boldsymbol{F}_{stick}\end{bmatrix} \tag{3.20}$$

where $\boldsymbol{F}_{slip}$ and $\boldsymbol{F}_{stick}$ are the forces at the contact points that are slipping and sticking, respectively and $\boldsymbol{F}_{slip_n}$ are the normal forces at the points i that are slipping,

$$\boldsymbol{F}_{slip} = \begin{bmatrix} f_{t_1} \\ f_{n_1} \\ . \\ . \\ . \end{bmatrix}, \qquad \boldsymbol{F}_{slip_n} = \begin{bmatrix} f_{n_1} \\ \vdots \end{bmatrix} \tag{3.21}$$

In Eq. (3.20) the matrix $S_c$ relates the normal forces of the slipping points to the tangential forces using the equality relation of Coulomb friction law,

$$S_c = \begin{bmatrix} -x_i\mu_i & 0 \\ 1 & \\ 0 & I \end{bmatrix} \tag{3.22}$$

where $x_i = {v_{t_i}}/{\|v_{t_i}\|}$ gives the direction of the contact point, $\mu_i = \mu_d$ is the dynamic coefficient of friction at point i, and I is an identity matrix.

Using dual property of the Jacobian matrix, the generalized active forces, **Γ** in Eq. (3.1), are related to the constraint forces as

$$\boldsymbol{\Gamma} = {J_c}^T \boldsymbol{F} = {J_c}^T S_c \begin{bmatrix} \boldsymbol{F}_{slip_n} \\ \boldsymbol{F}_{stick} \end{bmatrix} \tag{3.23}$$

Based on the dual property of the Jacobian matrix, the force constraint in Eq. (3.23) may be written as a velocity constraint,

$$0 = \begin{bmatrix} \boldsymbol{v}_{stick} \\ \boldsymbol{v}_{slip_n} \end{bmatrix} = {S_c}^T J_c \dot{\boldsymbol{q}} = J_I \dot{\boldsymbol{q}}_{\boldsymbol{I}} + J_D \dot{\boldsymbol{q}}_{\boldsymbol{D}} \tag{3.24}$$

where $\boldsymbol{v}_{stick}$ refers to both the normal and the tangential velocity components of the points that are sticking, $\boldsymbol{v}_{slip_n}$ refers to only the normal velocity components of the points that are slipping, and $\dot{\boldsymbol{q}}_{\boldsymbol{D}}$ and $\dot{\boldsymbol{q}}_{\boldsymbol{I}}$ are the dependent and independent generalized speeds. Now $\dot{\boldsymbol{q}}$ and $\ddot{\boldsymbol{q}}$ can be expressed as

$$\dot{\boldsymbol{q}} = \begin{bmatrix} \dot{\boldsymbol{q}}_{\boldsymbol{D}} \\ \dot{\boldsymbol{q}}_{\boldsymbol{I}} \end{bmatrix} = \begin{bmatrix} -{J_D}^{-1} J_I \\ I \end{bmatrix} \dot{\boldsymbol{q}}_{\boldsymbol{I}} = K \dot{\boldsymbol{q}}_{\boldsymbol{I}} \tag{3.25}$$

and

$$\ddot{\boldsymbol{q}} = K \ddot{\boldsymbol{q}}_{\boldsymbol{I}} + \dot{K} \dot{\boldsymbol{q}}_{\boldsymbol{I}}, \qquad \dot{K} \dot{\boldsymbol{q}}_{\boldsymbol{I}} = \begin{bmatrix} -{J_D}^{-1} \left( \dot{S}_c^{\,T} J_c + {S_c}^T \dot{J}_c \right) \dot{\boldsymbol{q}} \\ 0 \end{bmatrix} \tag{3.26}$$

Substituting Eqs. (3.24) and (3.26) into Eq. (3.1) and pre-multiplying with $K^T$ yields

$$K^T AK\ddot{\boldsymbol{q}}_{\boldsymbol{I}} + K^T\left(A\dot{K}\dot{\boldsymbol{q}}_{\boldsymbol{I}} + \boldsymbol{b} + \boldsymbol{g}\right) = K^T {J_c}^T S_c \begin{bmatrix} \boldsymbol{F}_{slip_n} \\ \boldsymbol{F}_{stick} \end{bmatrix} + K^T G^T \boldsymbol{\gamma} \tag{3.27}$$

From Eqs. (3.24) and (3.25), it can be easily shown that

$$K^T {J_c}^T S_c = 0 \tag{3.28}$$

Hence, the reduced set of equations of motion are given by

$$K^T AK\ddot{\boldsymbol{q}}_{\boldsymbol{I}} + K^T(A\dot{K}\dot{\boldsymbol{q}}_{\boldsymbol{I}} + \boldsymbol{b} + \boldsymbol{g}) = K^T G^T \boldsymbol{\gamma} \tag{3.29}$$

Thus, during contact Eqs. (3.29), (3.25) and (3.26) are used to integrate the states of the dynamic system.

# Chapter 4

## Operational Space Control

The idea behind operational space control is to abstract away from the generalized coordinates of the system and plan a trajectory in a coordinate system that is directly relevant to the task that we wish to perform. The robot can choose any joint space configuration it desires, independent of any operational space parameters. Once we task a robot to "move to point A (in operational space)," we have just built an implicit constraint on the robot's joint space such that it must use its kinematics to move to point[21].

The dynamic performance of a manipulator is strongly dependent on the inertial and acceleration characteristics that are perceived at its end effector.

### 4.1 Operational Space Equation Formulation

The joint space equation of motion is written as:

$$A\ddot{\boldsymbol{q}} + \boldsymbol{b}(\boldsymbol{q}, \dot{\boldsymbol{q}}) + \boldsymbol{g}(\boldsymbol{q}) = \boldsymbol{\Gamma} + G^T\boldsymbol{\gamma} \tag{4.1}$$

where $A$ is the mass matrix, $\boldsymbol{q}$,$\dot{\boldsymbol{q}}$ $and$ $\ddot{\boldsymbol{q}}$ are the generalized coordinates, speeds and accelerations, $\boldsymbol{b}(\boldsymbol{q}, \dot{\boldsymbol{q}})$ is the vector of centrifugal and Coriolis Joint forces and $\boldsymbol{g}(\boldsymbol{q})$ is the vector of gravity forces. $\boldsymbol{\Gamma}$ is the vector of generalized active forces, $\boldsymbol{\gamma}$ is the vector of Motor torques and $G^T$ is the vector of Gear Ratios.

We will look at three ways to find out the Motor torques $\boldsymbol{\gamma}$, depending on the nature of the Task Jacobian $J_x$ which is associated with the end-effector.

*4.1.1 If the Task Jacobian $J_x$ is invertible*

Using Eq. (3.29) as our general equation of motion while implementing operational space control

$$K^T AK\ddot{\boldsymbol{q}}_{\boldsymbol{I}} + K^T(A\dot{K}\dot{\boldsymbol{q}}_{\boldsymbol{I}} + \boldsymbol{b} + \boldsymbol{g}) = K^T G^T \boldsymbol{\gamma} \tag{4.2}$$

In operational-space control, we intend to execute trajectories or forces given in the coordinate system of the actual task.

We can represent generalized speeds and accelerations in terms of operational space velocities and accelerations, i.e.

$$\boldsymbol{v} = J_x\dot{\boldsymbol{q}}, \qquad \dot{v} = \dot{J_x}\dot{\boldsymbol{q}} + J_x\ddot{\boldsymbol{q}} \tag{4.3}$$

We can rewrite eq. (4.2) as:

$$\ddot{\boldsymbol{q}}_{\boldsymbol{I}} + (K^T AK)^{-1}K^T(A\dot{K}\dot{\boldsymbol{q}}_{\boldsymbol{I}} + \boldsymbol{b} + \boldsymbol{g}) = (K^T AK)^{-1}K^T G^T \boldsymbol{\gamma} \tag{4.4}$$

Using eq. (4.3), we can write eq. (4.4) as:

$$J_x{}^{-1}(\dot{\boldsymbol{v}} - \dot{J_x}\dot{\boldsymbol{q}}) + (K^T AK)^{-1}K^T(A\dot{K}\dot{\boldsymbol{q}}_{\boldsymbol{I}} + \boldsymbol{b} + \boldsymbol{g}) = (K^T AK)^{-1}K^T G^T \boldsymbol{\gamma} \tag{4.5}$$

or;

$$\gamma = ((K^T AK)^{-1}K^T G^T)^{-1}(J_x{}^{-1}(\dot{\boldsymbol{v}} - \dot{J_x}\dot{\boldsymbol{q}}) + (K^T AK)^{-1}K^T(A\dot{K}\dot{\boldsymbol{q}}_{\boldsymbol{I}} + \boldsymbol{b} + \boldsymbol{g})) \tag{4.6}$$

where,

$$\dot{\boldsymbol{v}} = \dot{\boldsymbol{v}}_{\boldsymbol{des}} + k_v(\boldsymbol{v}_{\boldsymbol{des}} - \boldsymbol{v}) + k_p(\boldsymbol{x}_{\boldsymbol{des}} - \boldsymbol{x}) \tag{4.7}$$

Eq. (4.7) is a basic PD control signal where, $\dot{\boldsymbol{v}}_{\boldsymbol{des}}, \boldsymbol{v}_{\boldsymbol{des}}\ and\ \boldsymbol{x}_{\boldsymbol{des}}$ are the desired end-effector acceleration, desired end-effector velocity and desired end-effector position. $k_v$ and $k_p$ are the velocity and position gains where $k_v$ can be written as $k_v = \sqrt{(k_p)}$.

Eq. (4.6) is the basic operational space equation to calculate motor torques $\boldsymbol{\gamma}$. This form of the equation requires inverting the Jacobian the matrix which can often be non-square. Hence, we will see another approach to form the operational space equation if the Jacobian is not a square matrix.

*4.1.2 If the Task Jacobian $J_x$ is not invertible*

Multiplying eq. (4.4) with the Task Jacobian $J_x$

$$J_x\ddot{\boldsymbol{q}}_{\boldsymbol{I}} + J_x(K^TAK)^{-1}K^T(A\dot{K}\dot{\boldsymbol{q}}_{\boldsymbol{I}} + \boldsymbol{b} + \boldsymbol{g}) = J_x(K^TAK)^{-1}K^TG^T\boldsymbol{\gamma} \quad (4.8)$$

Using eq. (4.3) to substitute for $J_x\ddot{\boldsymbol{q}}_{\boldsymbol{I}}$

$$\dot{\boldsymbol{v}} - \dot{J}_x\dot{\boldsymbol{q}} + J_x(K^TAK)^{-1}K^T(A\dot{K}\dot{\boldsymbol{q}}_{\boldsymbol{I}} + \boldsymbol{b} + \boldsymbol{g}) = J_x(K^TAK)^{-1}K^TG^T\boldsymbol{\gamma} \quad (4.9)$$

where,

$$\dot{\boldsymbol{v}} = \dot{\boldsymbol{v}}_{\boldsymbol{des}} + k_v(\boldsymbol{v}_{\boldsymbol{des}} - \boldsymbol{v}) + k_p(\boldsymbol{x}_{\boldsymbol{des}} - \boldsymbol{x}) \quad (4.10)$$

Equation (4.10) is a basic PD control signal.

The equation then becomes,

$$\boldsymbol{\gamma} = (J_x(K^TAK)^{-1}K^TG^T)^{-1}\left(\dot{\boldsymbol{v}} - \dot{J}_x\dot{\boldsymbol{q}} + J_x(K^TAK)^{-1}K^T(A\dot{K}\dot{\boldsymbol{q}}_{\boldsymbol{I}} + \boldsymbol{b} + \boldsymbol{g})\right) \quad (4.12)$$

With the second approach, the problem of inverting the non-square Jacobian matrix is solved provided that the term $(J_x(K^TAK)^{-1}K^TG^T)$ is invertible.

*4.1.3 If $(J_x(K^TAK)^{-1}K^TG^T)$ is not a square matrix*

If the term $(J_x(K^TAK)^{-1}K^TG^T)$ is not a square matrix, it cannot be inverted. To make this product a square matrix, an extra row to the Jacobian matrix is added to make the number of rows in the Jacobian equal to the number of columns in the Gear Ratio matrix. The extra row that is added to the Jacobian, performs a one to one mapping of the Cartesian velocities.

*4.1.4 Using the Dynamically Consistent Generalized Inverse of Jacobian*

If the Task Jacobian $J_x$ is not invertible, we can calculate its Dynamically Consistent Generalized Inverse [22], $\bar{J_x}$

$$\bar{J_x} = (K^TAK)^{-1}J_x^T\Lambda \quad (4.13)$$

Where $\Lambda$ is the operational space inertia matrix, given as:

$$\Lambda = J_x^{-T}(K^T A K)J_x^{-1} \tag{4.14}$$

# Chapter 5

# Results

This section presents the results of our hybrid dynamic model along with simulation techniques.

## 5.1 Simulation Technique

The hybrid simulation technique implemented for this work uses Matlab's ode45, which is an adaptive Runge–Kutta integrator based on the Dormand–Prince method. The results in this section were simulated in Matlab on an Intel(R) Core(TM) i7-4700MQ CPU with 2.4 GHz processor and 8 GB RAM.

## 5.2 Simulation Example

The planar model has 4 links and 6 Degrees of Freedom. Link 1 represents the foot, Link 2 represents the Tibia, Link 3 represents the Femur and Link 4 represents the rest of the body modelled as a circle with A, B, C and D denoting the centre of mass for each link and E, F, G, H and I (any point on the body) are the points being considered that will be in contact/impact. COM is the centre of mass for the whole system. The motors are placed at the heel(T1), knee(T2) and hip joints(T3).

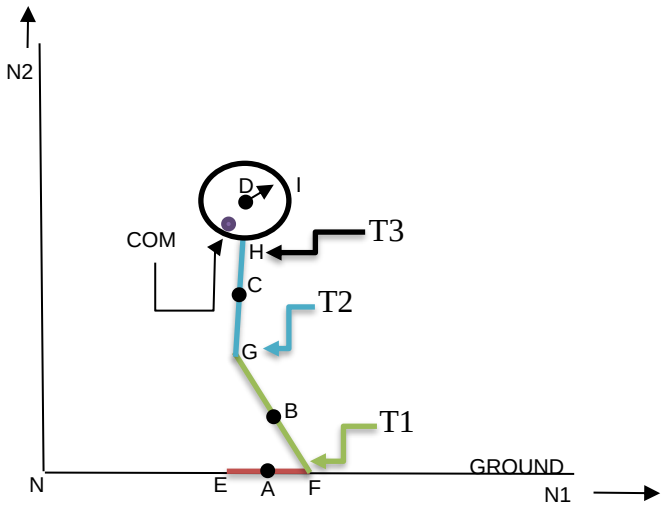


Figure 5-1: Planar Model of a Leg

The configuration of the model is given by a set of generalized coordinates

$$q = [q_1\, q_2\, q_3\, q_4\, q_5\, q_6]^T \tag{5.1}$$

where $q_1$ and $q_2$ are the translational coordinates. $q_3$ , $q_4$ , $q_5$ and $q_6$ are the revolute coordinates. $q_1$ and $q_2$ are the location of the point E in the x and y direction. $q_3$ is the rotation of body A with respect to the ground. $q_4$ is the rotation of body B with respect to body A . $q_5$ is the rotation of body C with respect to body B. $q_6$ is the rotation of body D with respect to body C . The dimensions of the bodies are denoted by L1, L2, L3 and L4. The initial impact with the contact surface will be assumed at points E and F.

Below are the initial conditions and the length and mass properties that were used in this simulation.

$$q = [4\ \ 0.01\ \ 0\ \ 2.0944\ \ -0.4363\ \ -0.6981]^T$$

$$L1 = 0.5\ m, L2 = 1\ m, L3 = 1.05\ m, L4 = \ 0.4\ m$$

$$MA = 0.816\ kg, MB = 2.58\ kg, MC = 8.496\ kg, MD = 24\ kg$$

## 5.3 Energy and Torque Plots

The energy plots shown below validate the results we have obtained. The first plot shows the change in the energy after the first impact event has occurred. We observe that while the model is still in the air, energy remains constant and as soon as an impact occurs, energy decreases.

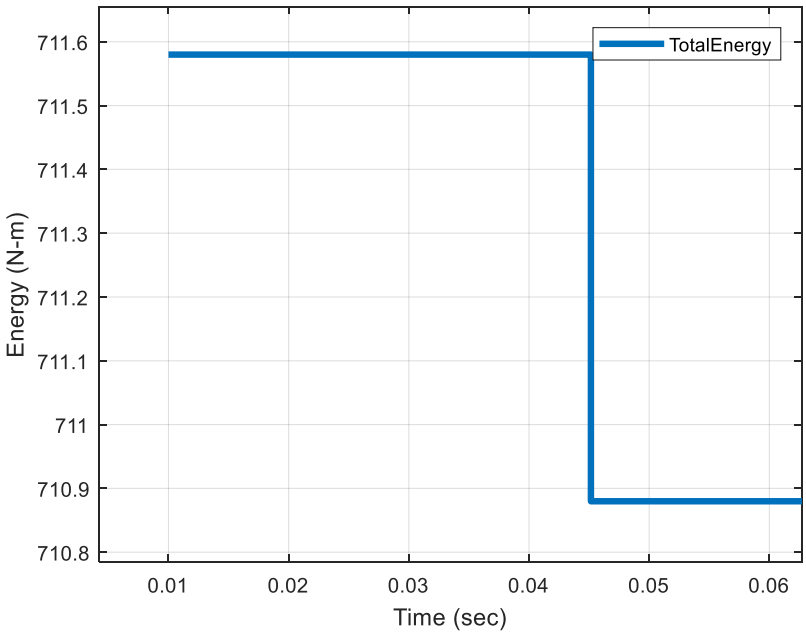


Figure 5-2: Total energy after First Impact event

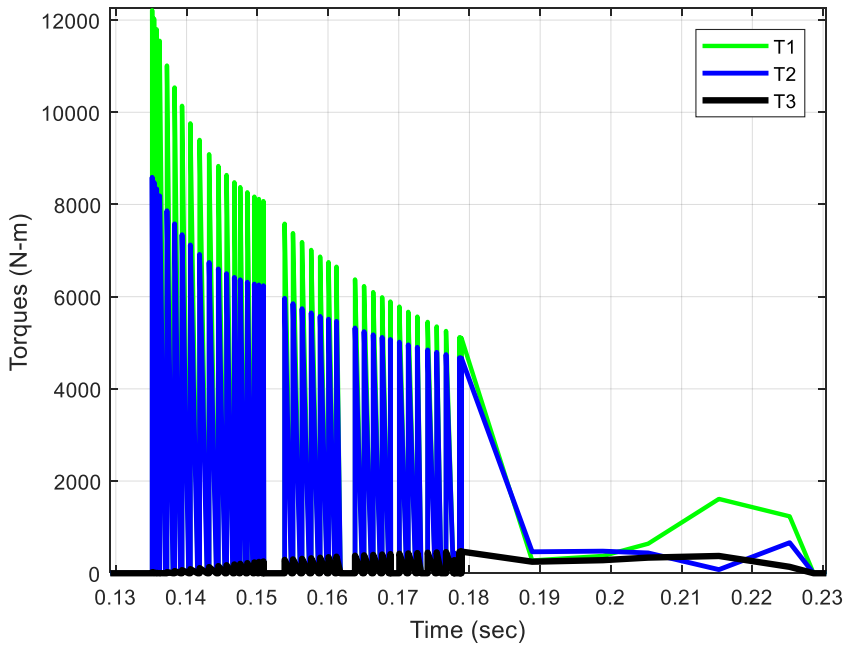


Figure 5-3: Torques leading up to the lift

Figure 5-3 shows the torque values that lifts the foot off of the ground. We observe from the plot that the we start calculating torques when the whole foot is in contact with the ground. We use 2 values for the gain $K_p$ depending on if we have a one-point contact or two-point. This impulse-like behaviour of the torques is due to the fact that we are switching from a two-point contact to a one-point contact. We observe that as soon as the whole foot lifts off from the ground, the controller is switched off. Since we are not bounding the torques, we see these high values of the motor torques being applied.

Figure 5-4 shows the total energy during the simulation. We have work done by the actuators in orange, the total energy including the work done by the actuators in blue and the kinetic energy in yellow. We can see that the total energy remains constant throughout the simulation and hence validates the dynamic consistency of our model.

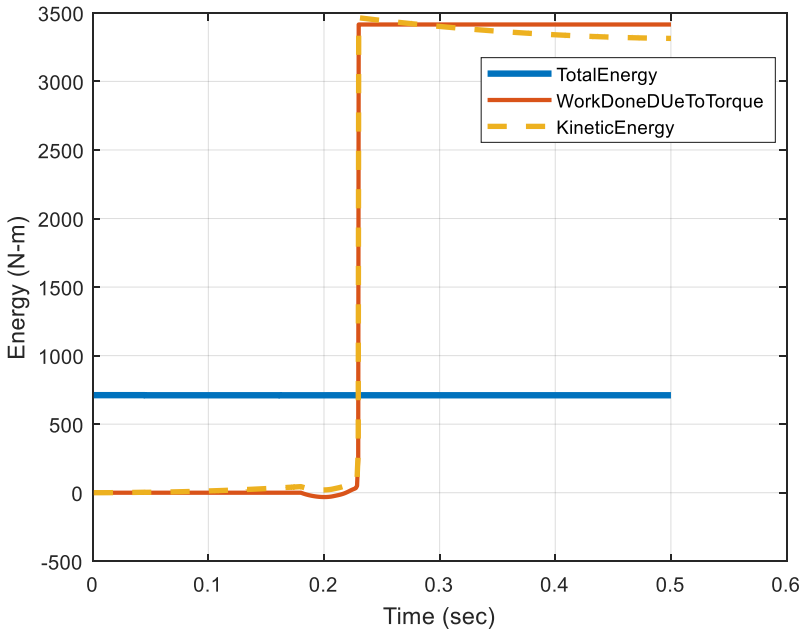


Figure 5-4: Total Energy Plot

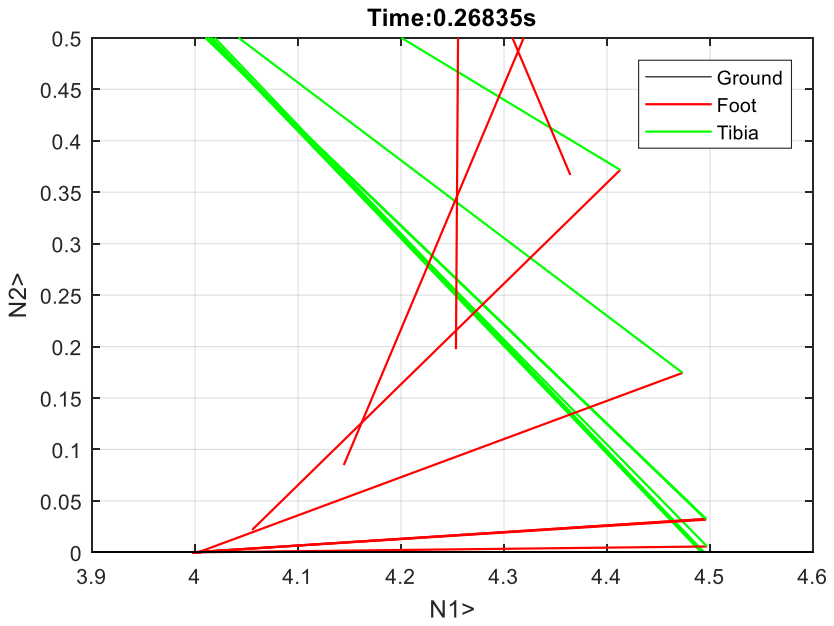


Figure 5-5: Motion Capture of the foot lifting off the ground

Figure 5-5 shows us how the heel first comes out of contact and then the toe leaves the contact surface.

Figure 5-6 shows us a motion capture of our simulated model. Our links are not bound by any angle constraints hence once they leave the contact surface, they move without any restraint.

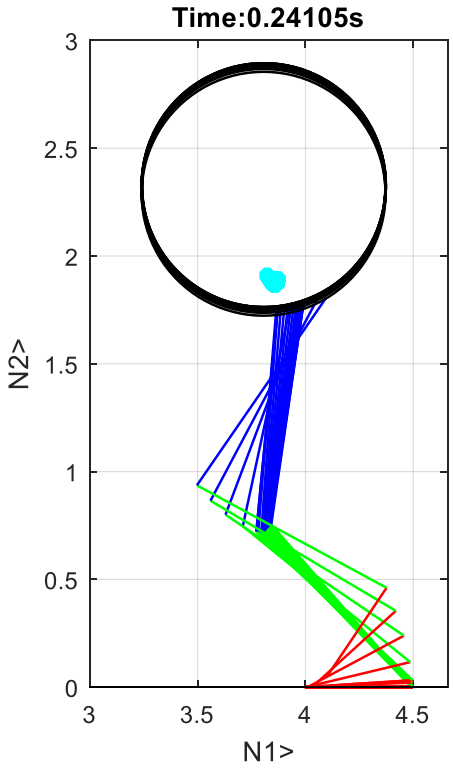


Figure 5-6: Motion Capture of the whole model

# Chapter 6

## Conclusion

Using the impact and contact analytical framework, we were able to establish a sound impact and contact model. Using the operational space controller, we were able to achieve a proper lift off the foot from the ground.

The next application using the operational space controller would be to keep the orientation of the model fixed to achieve not only a proper lift off from the ground, but also a proper landing of the dynamic model. We will also put in bounds for our actuator torque values.

## References


1. Rodriguez, A (2014). Dynamic Simulation of Multibody Systems in Simultaneous Indeterminate Contact and Impact with Friction (Doctoral dis*sertation).* Retrieved from https://uta-ir.tdl.org/uta-ir/handle/10106/24399.
2. Bernard Brogliato, 'First Order Impact Dynamics: Darboux-Keller's Shock Eqations", *Nonsmooth Mechanics: Models, Dynamics and Control*, pp 200, Feb 2016.
3. Y. Gonthier, J. McPhee, C. Lange, and J.-C. Piedboeuf, "A regularized contact model with asymmetric damping and dwell-time dependent friction," Multibody System Dynamics, vol. 11, no. 3, pp. 209–233, Apr. 2004.
4. I. Sharf and Y. Zhang, "A contact force solution for non-colliding contact dynamics simulation," Multibody System Dynamics, vol. 16, no. 3, pp. 263–290, Oct. 2006.
5. G. Gilardi and I. Sharf, "Literature survey of contact dynamics modeling," Mechanism and Machine Theory, vol. 37, no. 10, pp. 1213–1239, Oct. 2002
6. B. Brogliato, Nonsmooth Mechanics: Models, Dynamics and Control. Springer-Verlag London Ltd., 2nd ed., 1999.
7. R. Leine and N. Van de Wouw, Stability and convergence of mechanical systems with unilateral constraints. Springer Science & Business Media, 2007, vol. 36.
8. J. Keller, "Impact with friction," Journal of Applied Mechanics, Transactions ASME, vol. 53, no. 1, pp. 1–4, Mar. 1986.
9. Stronge, W.: "Smooth dynamics of oblique impact with friction," International Journal of Impact Engineering, vol. 51, pp. 36–49, Jan. 2013.
10. P. Bergés and A. Bowling, "Rebound, slip, and compliance in the modeling and analysis of discrete impacts in legged locomotion," Journal of Vibration and Control, vol. 17, no. 12, pp. 1407–1430, Dec. 2006.
11. S. Djerassi, "Stronge's hypothesis-based solution to the planar collision-with-friction problem," Multibody System Dynamics, vol. 24, no. 4, pp. 493–515, Dec. 2010.
12. C. d. Coulomb, "Th´eorie des machines simples, en ayant ´egard au frottement de leurs parties, et la roideur des cordages," Pi´ece qui a report´e le Prix double de l'Acad´emie des Sciences pour l'ann´ee, pp. 163–332, 1785.
13. S. Djerassi, "Collision with friction; Part B: Poisson's and Stronge's hypotheses,"Multibody System Dynamics, vol. 21, no. 1, pp. 55–70, Feb. 2009.
14. P. Song, P. Krauss, and P. Dupont, "Analysis of rigid-body dynamic models for simulation of systems with frictional contacts," ASME Journal of Applied Mechanics, vol. 68, no. 1, pp. 118–128, Jun. 2000.
15. B. Brogliato, A. Ten Dam, L. Paoli, F. G´enot, and M. Abadie, "Numerical simulation of finite dimensional multibody nonsmooth mechanical systems," Applied Mechanics Reviews, vol. 55, no. 2, pp. 107–149, Mar. 2002.
16. C. Glocker and C. Studer, "Formulation and preparation for numerical evaluation of linear complentarity systems in dynamics," Multibody System Dynamics, vol. 13, no. 4, pp. 447–463, May 2005.
17. D. Haessig and B. Friedland, "On the modeling and simulation of friction," American Control, vol. 113, no. 3, pp. 354–362, Sep. 1991.
18. J. Moreau, "Numerical aspects of the sweeping process," Computer Methods in Applied Mechanics and Engineering, vol. 177, no. 3, pp. 329–349, May 1999.
19. D. Flickinger and A. Bowling, "Simultaneous oblique impacts and contacts in multibody systems with friction," Multibody System Dynamics, vol. 23, no. 3, pp. 249–261, Mar. 2010.
20. A. Chatterjee, A. Rodriguez and A. Bowling, "Analytical solution for planar indeterminate impact problems using an energy constraint," Multibody System Dynamics, vol. 42, no. 3, pp. 347-379, Mar. 2018.
21. https://studywolf.wordpress.com/2013/09/17/robot-control-4-operation-space-control/
22. O. Khatib, "A unified approach to motion and force control of robot manipulators: The operational space formulation International Journal of Robotics and Automation, 3 (1) (1987), pp. 43-53

## Biographical Information

Gurashish Singh was born in New Delhi, India in 1991. He received a B.E. in Mechatronics Engineering from Manipal Institute of Technology, Manipal University in 2014 and an M.S. in Mechanical Engineering from The University of Texas at Arlington in 2018.

His areas of interest include Dynamics, Controls and Robotic Systems. His favourite hobbies are reading and playing football.